Investigation of Linear and Nonlinear Variations of Radon, Total Electron Content and Meteorological Variables by Earthquakes: ARIMA and Monte Carlo Modeling

hemn salh (hemn.salh@koyauniversity.org)
Firat University: Firat Universitesi https://orcid.org/0000-0002-2367-2980
Fatih Külahcı
Firat University: Firat Universitesi
Marjan Mohammed Ghafar
Firat University: Firat Universitesi

Research Article

Keywords: Radon gas, Total Electron Content, Earthquake prediction, ARIMA, Monte Carlo Simulation

Posted Date: March 16th, 2022

DOI: https://doi.org/10.21203/rs.3.rs-1381223/v1

Abstract

An Autoregressive Integrated Moving Average (ARIMA)-Monte Carlo Simulation (MCS) is proposed to analyze and model anomalies caused by earthquakes in the atmosphere and ground gases along the North Anatolian Fault Zone (NAFZ)-Turkiye. Earthquakes, Soil Radon Gas and Total Electron Content (TEC) show anomalies simultaneously. Positive correlations are observed among these three variables. Similarly, positive correlations are also observed among Rn-Meteorological-Atmospheric triple variables. The proposed ARIMA model and MCS for the Rn-TEC-Earthquake relations of the measured data gave statistically significant results. This model and simulation gave also significant peaks for the effects of micro earthquakes, which are more difficult to detect than large earthquakes, especially on the ionospheric TEC.

Introduction

The formations of the earthquake are one of the most complex geological events that exist on the surface of the earth as a result of many parameters effects. Often, soil radon (^{222}Rn) gas adjustment is not just sufficient due to many factors that affect the surface of the earth such as the soil structure, air pressure, humidity, environmental warmings, weather gauge, and land penetrability (Külahci et al. 2009). The earthquake is a discontinuous movement across poor zones that are fractures in the crust of the earth (MILNE 1910). An earthquake is the product of a vast energy amount that travels for thermal energy, seismic wave energy, plastic deformation energy then for earthquake only seismic wave is considered. For the simplicity of the earthquake energy estimation, the principle of magnitude has been added (Pulinets 2018). The precursors of an earthquake are actions in the physical, chemical, and other characteristics of the composites that make up the crust, resulting from the deposition of stress in the crust which contribute to the formation of various anomaly types in the earthquake regions, which are observed by seismologists and serve as a base for earthquake forecasts (Pulinets 2018).

Radon is an uncolored gas and its half-life is (3.8) days. ^{222}Rn is the heaviest noble gas and the more stable isotope that occurs naturally as a radium decay product (Venkatanathan et al. 2017). The main source of Rn is Ra in the Earth's crust, and at least 80% of the Rn released into the atmosphere is in the Earth's upper several meters, in rocks and dust; the radium level is mostly equivalent to that of uranium. The global mean concentration of soil for ^{238}U is around 24 Bq/kg. The amount of radium and uranium in the soil ranges according to rock and mineral varieties (Nazaroff 1992 and Beach 1984). Investigation into Rn emission concentrations from the surface of the earth has effects in several different fields of earth and atmospheric sciences. Rn and its progenies are used to measure processes from atmospheric source tracing and transportation (in and among the stratosphere and the troposphere). Stability of air mass and time of vertical motion, rates of removal, and aerosol residency times, continental dust air mass sources, and air-sea interface gas exchange have been studied. A detailed understanding of the variables and mechanisms governing the levels of Rn emanation of rocks, minerals and soil are important for all these studies (Baskaran 2011). Due to low solid diffusing coefficients (10^{-25}-10^{-27}

m^2/s) in a solid grain, Rn atoms cannot escape the mineral grain. It is generally accepted that as parent Ra undergoes radioactive decay, as a result of the recoil and Rn escapes from mineral grain. The decay of Ra generates Rn atoms that escape grains, often because of recoil and because of the space within grains. They can be transferred due to diffusion (the molecular diffusion coefficient of air and water) through the processes of Rn removal from the subsurface and transportation to the atmosphere subsequently (Baskaran 2016).

^{222}Rn has been using for the earthquake of prediction (Rikitake 1968; King 1978; Birchard and Libby 1980), utilization ^{222}Rn for monitoring seismic activities started with the (M 5.2) earthquake in Tashkent. The research area was taken under consideration about 6 years before the Tashkent earthquake (Ulomov et al. 1967). Hence, the data shows also amounts of radon growth prior to the earthquake. The vibration of the Earth's crust in numerous portions of the World has been the leader of new ways of earthquake predictions (Külahcı et al. 2014). These prediction fields contain various methods with important effects. The magnetic region, compressing, decline, velocity wave of seismic, shell resistance, slide down, gravitational effects and radon measurements are such methods, and this record shows that earthquakes can cause rise in radon levels. Preceding earthquake Chamoli Indian 1999, there was high variation in soil radon gas (Virk and Walia 2001; Singh et al. 2019), After North Indian earthquake 1997 (M 5.4), radon gas is measured abnormally due to mensuration of water source underground. Comparably radon gas is higher than in ordinary soils (Viñas et al. 2007). The amount of radon emitted into the atmosphere from the earth's crust is usually small, but the fault lines in geothermal resources in uranium and radon anomalies are observed before the formation of volcanic eruptions and earthquake events (Külahcı et al. 2009).

At altitudes of 60 to 1100 km, the ionosphere is the portion of the atmosphere where ions and free electrons reflect an insignificant amount of electromagnetic waves (Inyurt et al. 2019). Atmospheric TEC represents the number of free electrons along $1m^2$ of ray path (Arikan et al. 2007). TEC measurement is used directly to analyze the nature of the ionosphere, and while it is measured by the TECU unit, and 1 TECU is equivalent to 10^{16} electron.m^{-2} (Géodésique 1999). TEC is estimated through vertical TEC; free electron content is estimated in the slant line between the recipient and the satellite is determined on the recipient's zenith and Slant Total Electron Content (STEC) (Langley 2002). Geomagnetic influences, solar interference, diurnal and seasonal effects and earthquakes are influenced by the ionosphere, generating anomalies in the ionosphere (Inyurt et al. 2019). The TEC is an important research parameter for the correlation between pre-earthquake and seismic events since it can explain changes in the ionosphere due to these activities. This is due to seismic and pre-earthquake events in the Earth's crust that produce stress in rocks. The positive charge of rocks on the earth's crust is caused by stresses. If the positive charges are collected on the outer surfaces of the rocks, they generate a potential difference that in turn produces a flow of charges, which can migrate rapidly, and therefore, is far from their original location. Under the impact of the electric field lines between the Earth's crust and the bottom of the ionosphere, the charges shift upward. They reach the bottom of the ionosphere as a result of disturbance with the electrons balance in the ionosphere (Viti et al. 2013). Such a disturbance was seen in the total electron

content, and TEC a potential candidate for earthquake precursor is possible, if TEC disruptions could be used as a guide to the earthquake monitoring, where these disturbances could be used as part of an earthquake forecasting mechanism that would strengthen earthquake alarm services, and hence, protecting countless lives in turn (Hammerstrom and Cornely 2016). Ionospheric TEC also in response to geomagnetic influences, solar interference, seasonal and diurnal effects, and earthquakes, which induce anomalies in the ionosphere (Namgaladze et al. 2012; Li and Parrot 2018). In more than twenty countries, ionospheric variations have been observed as earthquake precursors (Liu et al. 2010; Li and Parrot 2018).

The aim of this study is to model the output of soil radon gas, which is directly related to the seismic activity, and the changes in the ionospheric TEC, taking into account the earthquakes and relate them using Monte Carlo Simulation. While examining this relationship, some meteorological variables are also included in the calculations. According to the results obtained, significant findings are obtained on the co-change of TEC-Rn-Earthquake triad.

Study Area And Data Analysis

Turkiye is one of the most seismic activity places and also the active North Anatolian Fault Zone (NAFZ) seismically affects the northern part as well as a dextral strike-slip movement with a surface rupture of about 1,600 km long (Allen 1969; Inyurt et al. 2019), located on the eastern side of the North Anatolian Fault as a study field, which is an important region as for the regard to construction and future growth as a result of earthquake events from 1942 and 1943 with magnitudes (7.6 and 7.2) (Allen 1969; Inyurt et al. 2019). The study area is Yolkonak in Tokat Province-Turkiye. This area is situated along one of the main fault zone in Turkiye, which is the NAFZ. The NAFZ is in the mid-Black Sea Region and Tokat province. It extends between (longitude 36^{o}.89443, latitude 40^{o}.53932), and north latitude. Scale topographical sheets are shown in Figure 1.

Figure 1

The ^{222}Rn time series data are gained from Republic of Turkiye Ministry of Interior Disaster and Emergency Management Presidency (AFAD) (https://en.afad.gov.tr/). In this study, soil radon is measured by an alpha particle detector at about 1 m depth in soil with 15 minutes' interval from 4 March 2007 to 10 February 2010. The detector is model 611 Alpha Meter, manufactured by Alpha Nuclear Corporation, Canada. Take the form of a 400 mm^2 silicone diffuse cross-detector housing in stainless steel that is covered from an aluminum Mylar (Thomas et al. 1992). The detector has a sensing surface of 450 squared millimeters. It is sealed behind a thin opaque film or membrane since this detector requires a dry, dark environment to work. The film is 0.25 mm aluminized Mylar, and therefore of sufficiently low density for effective passage of alpha particles, besides water vapor and light.

To study the effect of meteorological parameters on the ^{222}Rn at the study period, the daily mean soil temperature at 10 cm, 20 cm, and 50 cm depths as well as daily mean steam pressure (hPa), wet bulb temperature and dry bulb temperature are obtained from T.C. Meteorology General Directorate

(https://www.mgm.gov.tr/eng/forecast-cities.aspx). The earthquake data are given by Bogazici University, Kandilli Observatory and the Research Institute for Earthquake (www.koeri.boun.edu.tr/sismo/2/earthquake-catalog). Moreover, this study utilized the regularized estimation method for GPS measurements to obtain VTEC values for three mid-latitude stations, Ankara, (39.53N, 32.45E), Istanbul, (41.06N, 29.01E), Gebze, (40.47N, 29.27E) through IONOLAB-Ionosphere Research Laboratory (http://www.ionolab.org/index.php?page=index&language=en).

Results And Discussion

Autoregressive Integrated Moving Average (ARIMA) Model and Monte Carlo Simulation (MCS)

The Autoregressive Integrated Moving Average (ARIMA) stochastic models are used for forecasting. The model of the time series determines how many previous terms need to be taken into account and represented as the series of various models. The MATLAB software is used to detect possible radon data perturbations due to seismic activities in the study area. It provides a workspace to define the best ARIMA model by Monte-Carlo simulations application to predict further radon time series. After Rn data importation, 80% of the data is used as the train data set to find the best ARIMA model, while the 20% of the data was used for evaluating the Monte-Carlo simulation data prediction. ARIMA model can only be implemented if the data is stationary (Salh et al. 2021). The Dickey-Fuller Test showed that the train data set of Rn is not stationary, because its t-static is greater than the critical value, thus the Rn train set is differenced by one degree. The autocorrelation functions (ACF) and the partial autocorrelation function (PACF) prevail that the data is stationary. Besides, ACF and PACF plots help to determine the autoregressive p and moving average q orders. ACF, PACF plots of the differentiated data for 20 lags at significance level 0.05 confirm the stationarity of the data as can be seen in Fig. 2. ARIMA (p, d, q) is applied initially to train data. Then ARIMA (4,1,13) is chosen model of time series with the following equation:

$$(1 - \varphi_1 \mathrm{L} - \cdots - \varphi_4 L^4)(1 - \mathrm{L}) y_t = C + (1 + \theta_1 \mathrm{L} - \cdots - \theta_{13} L^{13}) \epsilon_{\backslash \mathrm{varvec}t} \quad (1)$$

where C is a constant, φ and $\theta$are the parameters of the model, and ϵ_t is the error at time *t*.

The histogram of the residuals of the model is presented in Fig. 2 which demonstrates normal distribution. The goodness of the residues of the fitted model is checked. It is observed that the residues are naturally distributed and not correlated as shown in Fig. 2. The Quantile-quantile plot of the residuals of the model is presented in Fig. 2. Despite a few differences in the tail, it can be shown that there seem to be abnormalities. The value of the normal distribution merges with the value of both residues, which suggest that ARIMA (4,1,13) model is adequate.

Figure 2

MCS is a mathematical method for statistical analysis and decision making. It is used effectively in many areas, such as atomic and high energy physics, nuclear energy, environment, engineering, research and growth, transporting (Abdolhamidzadeh et al. 2010; Zhao et al. 2011; Aalizadeh et al. 2019). It indicates the good and worst cases in all possible outputs, and illustrates all possible outcomes (such as the best and worst scenarios) with every possibility, as according to preferred method choices and works principle on determining the distribution of input/parameters that have variability and uncertainty with a probability distribution function (PDF) rather than a single value (Muhammad et al. 2021) and how to use these inputs for the distribution depending upon the number of uncertainly and the range of input values corresponding to those uncertainties, MCS provides different analyzes and according to a PDF, helps to give a set of different outcomes. The most logical and reliable approach to define uncertainties in a risk simulation work is the use of PDFs may be different like Gaussian, lognormal, uniform. The values are sampled by the randomly defined PDFs during MCS. The iteration of each sample set of is defined and the data is given as shown in this data sample. The MCS method shows not only what might happen, and also about the resultant PDFs about these results (Külahcı et al. 2020). Based on the ARIMA model the Monte-Carlo simulates 4 different paths and forecast 20% data time steps. It seems appropriate as in Fig. 3, where the Monte-Carlo forecast confidence bounds are also shown. The black line indicated is the average Monte-Carlo direction, red lines are lower and upper bounds, green lines is radon.

Figure 3

Non-Seismic associated soil-air radon gas concentration variations

The studied radon time series from March 2007 to February 2010 is shown in Fig. 4. It can be seen that the Rn concentration is not steady over time. From the beginning of March to November 2007 there is no significant change in the radon level, but, its concentration fluctuates around its mean (150 $Bq.m^{-3}$). Subsequently, the Rn level start to decrease gradually from the mid of October.

Figure 4

These variations in Rn concentration are not big compared to the end of 2007, where the Rn level recorded the minimum concentration at about 150 $Bq.m^{-3}$ during December 2007, January and February 2008. From March 2008, the Rn level gradually increase, and the maximum Rn concentration recorded in the spring this high concentration of Rn continue until the end of the summer, then gradually decreases until the winter of 2009 again. This seasonal cycle of soil air Rn concentration is visible in 2010 as well. This variation is a seasonal variation of Rn concentration. Vertical cracks in the clay are opened during the summer as a result of permeability increase and also in Rn concentrations (Lindmark and Rosen 1985). Due to stress of earthquakes in the earth's crust, there is a tremendous influence on Rn output. Changes in temperature between soil and air are also observed as associated with influencing the flux of Rn gas. It is commonly established from an air stream that Rn could be caught for activated charcoal at temperatures below − 10°C, cooled to liquid N_2 at -196°C on glass wool, soil CO_2 at -78.5°C. Although the

partial pressure of soil ^{222}Rn is very low in environmental conditions, Rn condenses at roughly − 150°C on the surface (Schery and Gaeddert 1982). Since the temperature of the air and the relative humidity of the air are inversely related, the surface soil moisture content is associated with increased temperature at warmer air and soil temperature. The levels of Rn emanation are predicted to be higher relative to colder temperatures (Baskaran 2016).

Variations of air pressure are soil Rn impacts of flux from the Earth's atmosphere (Schery and Gaeddert 1982). Pressure variations of 1–2 percent are correlated with frontal system route that are estimated to have derived in 20–60 percent differences in ^{222}Rn flux on the surface of the earth (Clements and Wilkening 1974). In most homes, where high levels of indoor Rn are found, these levels are ascribed to a simple difference in pressure between both the basement and the living space. In most residences high concentrations of indoor radon are detected, where these measurements are due to the slight difference in pressure between the living place and the basement, the influence is a suction effect because of the lower basement pressure. So, the air pressure in the surface is higher than the interface of the ground-air and consequently, Rn gas increment should be released into the air (Baskaran 2016).

Possible Seismic Activities linked soil-air radon gas concentration variations

The seismic activities in the study area, Tokat province, are recorded by Boğaziçi University, Kandili Observatory and the Research Institute for Earthquake during the period 2007–2010. It is found that, there are about 45 earthquakes of magnitude between 2.3M_L and 3.5M_L. During the period in which the radon data are measured, the seismic data is correlated with the concentration of the Rn level and the earthquakes with the time series as shown in Fig. 5.

Among them, 7 earthquakes occurred in 2007 and the strongest earthquake has M_L 3.2. There is a variation in the concentration of radon. Therefore, a seasonal variation occurred as mentioned earlier. In 2008, there were around fourteen earthquakes, among which three earthquakes had magnitude ML = 3.5, 3.5, and 3.4 in May and July, which are Gokal-Erbaa (Tokat) [South West 4.5 km], Mescitkoy-Almus (Tokat) [South 5.0 km], Sehitler- (Tokat) [South East 0.9 km], respectively. One month after these earthquakes, Rn level raised to its peak. Rn emission is related to changes in crust stress, when the earth's surface is relaxed or stretched it with results in earthquakes (Nazaroff and Nero 1988). In 2009, eighteen earthquakes took place and it has the most significant amount of Rn perturbations. Then the seismic distance location was not so far compared to others. In 2010, only two earthquakes were observed in the study area. The relationship between Rn and soil temperature is as shown in Fig. 5.

Figure 5

Geophysical and geochemical characteristics such as soil type, earthquakes, volcanic eruptions, underground drilling, gases releases, stresses, etc. affect the release of Rn from the surface of earth. Figure 5 shows that there is a relatively positive correlation between Rn changes and meteorological and atmospheric changes.

Monte Carlo Simulation Radon anomaly detection

As mentioned earlier, 80% of the radon data is used as the train data set to find the best ARIMA model, while the 20% for evaluating the MCS data prediction as shown in Fig. 6(a). During the MCS period, which is visualized by the pink line, there are almost eleven earthquakes in Fig. 6(b). At the beginning, there are two micro earthquakes with magnitudes 2.4 and 2.5. The Rn level did not vary significantly in response to these earthquakes because they are weak. Later, on 15th August 2009 after those earthquakes there were Rn anomalies, two peaks, and the line of Monte Carlo is parallel to that of Rn. The fourth earthquake was on 16th September 2009 with 2.9 magnitudes. The Rn concentration was not in response to the earthquake suddenly, but after several days the Rn level increased. In December 2009, there were four earthquakes after these earthquakes' Rn anomalies occurrence. The study area is located in the Anatolian Fault Zone and according to soil permeability, the Rn concentration rises as seismic fault lines, geothermal sources, uranium resources, and volcanic zones descriptions in theory. Soil radon ^{222}Rn emission naturally occurs from soil products from rock, soil, mineral, uranium mine tailings. The surface soil moisture content is associated with temperature increase, and in warmer air and soil temperatures, the levels of Rn emanation are higher relative to colder temperatures with the positive anomaly of Rn. It depends in particular, on the distance from the epicenter and the magnitude of the earthquake. The Rn anomaly peak intensity and width depend largely on the magnitude of the earthquake and the epicenter distance from the observation point.

Figure 6

Ionospheric Total Electron Content (TEC) perturbations

The TEC is an important research parameter in terms of the associations between TEC and pre-earthquake and seismic events, because it can explain changes in the ionosphere due to these activities as described in the literature. Then temporary radon with total electron for three stations in study area is shown in Figure 7. Interesting results are obtained in the triple analysis of earthquake-TEC and Rn anomalies Fig. 7. One can examine this figure from several basic sections point of view as an example. On the other hand, it is possible to increase the number of these segments (like the changes between 2007 and 2008), and when these changes are examined closely, it is seen that Earthquake-Rn-TEC gives anomalies almost simultaneously. It is clearly seen that the Rn gas concentration in the soil is discharged as a result of successive earthquakes in the section within the red column. Similar fill-discharge trends are observed as indicated in the blue and yellow columns. These anomalies tend to behave similarly for all three TEC stations.

Figure 7

The green line is the TEC in the Ista (Istanbul) station at the beginning, there is missing data until November 2007, which is the reason why the graph did not start from the origin. The purple line is the total electron content in the Tubi (Gebze) station during the already mentioned study period. The brown

line is the total content. The data of the electron in Anka (Ankara) station is discontinued in 2007 and continued in 2008.

The daily TEC value is confined within the confidence intervals of average and standard deviation to recognize, the boundaries by means and standard deviation of the following equation used 10 days before and 5 days after the observation day:

upper bound = MEAN + 2 STDEV, (2)

lower bound = MEAN − 2 STDEV, (3)

A TEC anomaly is detected five days before measuring 2.8 on the Richter scale on 16 September 2009 as in Fig. 8(a), where the anomaly of the three stations is the same due to the TEC irregularities at Ista station for 3 days before and after the earthquake fluctuation. Rn level with MCS is relatively suitable for prediction. On 7 December 2009, ML3.2 earthquakes was observed on the Richter scale as in Fig. 8(b), where TEC anomaly was observed three days before earthquake and after earthquake with TEC decreases. After this earthquake, Rn level increased before this earthquake Rn daily variation while some anomaly remained in Rn concentration. The Monte Carlo line is roughly parallel to the radon, but some time it is not reasonable. The last earthquake was 3.2 on the Richter scale on December 11, 2009, as in Fig. 8(b), but after two days, the level of TEC has increased for 3 days, which seems not related to earthquake. Hence, the abnormality in the TEC could be as a result of distance between the stations and the magnitude of the earthquake, because the energy of powerful earthquakes is much greater than the sum energy of many small earthquakes. The anomalous electron total may be a global positioning system (GPS) further from the epicenter that is absorbable as a result of strongly earthquakes. Here is a small earthquake.

Figure 8

The TEC abnormality indicates that under the impact of the generator force from around epicenter, there may be ambient noise in the pathway of GPS signals in the upper atmosphere (Tariq et al. 2019), which could outcome from solar and magnetic storms. Increased plasma density shows that significant anomalies in the ionosphere were usually related to the upward drift of the plasma around seismogenic regions (Shah et al. 2019).

Conclusions

The study investigated the Rn concentration variations in soil gas for about 4 years in Yolkonak/Tokat, Turkiye. It is observed that the concentration of soil radon at 1m depth have both seasonal and non-seasonal variations. Regarding the seasonal variations, the Rn concentration seems to be the least in winters, and it is higher in summer seasons due to the effects of the metrological parameters on the radon transportation normal mechanisms like diffusion. The non-seasonal variations (anomalies) has been detected by Monte Carlo simulations with increasing level of radon prior to micro earthquakes in

August 2009, and in December 2009. These anomalies are as the precursor to a possible earthquake in the North Anatolian Fault Zone (NAFZ). In some cases, the ionospheric total electron content variations appear related to the radon anomalies for example, before the 12 December 2009 earthquake total electron content crossed the upper boundaries simultaneously with the Rn level increments.

Unlike the interpretation of a single variable, the MCS method generates a PDF by adding all the available data to the calculations leading to the simulation optimization at the optimum level. When MCS is combined with the ARIMA model, high reliability statistical results with high reliability are obtained. It is seen that the use of the ARIMA-MCS method together in the interpretation of the data is beneficial for this research. We recommend the use of different artificial intelligence techniques in different studies.

In the analysis of soil Rn gas time series, significant positive increases are observed in Rn anomalies in hot seasons compared to cold seasons. These increases are due to the decrease in soil moisture in the hot season, the increase in the spaces between the soil pores, the increase of the spaces between the soil particles, the positive effect of the moon's gravitational movements, the less rainfall and the accompanying drought. Such seasonal changes are positively effective in Earthquake-Rn changes observations.

Air pressure changes have a direct effect on Rn changes on the surface. Rn, meteorological changes and atmospheric show a positive correlation between them. It can be said that there is a positive correlation between Rn-TEC-Earthquake.

References

1. Aalizadeh R, Nika M-C, Thomaidis NS (2019) Development and application of retention time prediction models in the suspect and non-target screening of emerging contaminants. Journal of Hazardous materials 363:277–285
2. Abdolhamidzadeh B, Abbasi T, Rashtchian D, Abbasi SA (2010) A new method for assessing domino effect in chemical process industry. Journal of Hazardous Materials 182:416–426. https://doi.org/https://doi.org/10.1016/j.jhazmat.2010.06.049
3. Allen CR (1969) Active Faulting in Northern Turkiye
4. Arikan F, Arikan O, Erol CB (2007) Regularized estimation of TEC from GPS data for certain midlatitude stations and comparison with the IRI model. Advances in Space Research 39:867–874. https://doi.org/10.1016/j.asr.2007.01.082
5. Baskaran M (2011) Po-210 and Pb-210 as atmospheric tracers and global atmospheric Pb-210 fallout: A Review. Journal of Environmental Radioactivity 102:500–513. https://doi.org/10.1016/j.jenvrad.2010.10.007
6. Baskaran M (2016) Physical, Chemical and Nuclear Properties of Radon: An Introduction. Radon: A Tracer for Geological, Geophysical and Geochemical Studies 1–14. https://doi.org/10.1007/978-3-319-21329-3_1

7. Beach L (1984) Exposure from the Uranium Series with Emphasis on Radon and Its Daughters, Report No. 77. National Council on Radiation Protection and Measurements. Journal of Nuclear Medicine 25:1273–1274
8. Birchard GF, Libby WF (1980) Soil radon concentration changes preceding and following four magnitude 4.2–4.7 earthquakes on the San Jacinto Fault in southern California. Journal of Geophysical Research: Solid Earth 85:3100–3106
9. Clements WE, Wilkening MH (1974) Atmospheric pressure effects on 222Rn transport across the Earth-air interface. Journal of Geophysical Research (1896-1977) 79:5025–5029. https://doi.org/https://doi.org/10.1029/JC079i033p05025
10. Demir G, Aytekin M, Akgun A (2014) Landslide susceptibility mapping by frequency ratio and logistic regression methods: an example from Niksar–Resadiye (Tokat, Turkey). Arabian Journal of Geosciences 2014 8:3 8:1801–1812. https://doi.org/10.1007/S12517-014-1332-Z
11. Géodésique des sciences naturelles. C (1999) Mapping and predicting the Earth's ionosphere using the Global Positioning System
12. Hammerstrom JA, Cornely P-RJ (2016) Total Electron Content (TEC) Variations and Correlation with Seismic Activity over Japan. https://doi.org/10.22186/JYI.31.4.13-16
13. Inyurt S, Peker S, Mekik C (2019) Monitoring potential ionospheric changes caused by the Van earthquake (<i>M</i>_w7.2). Annales Geophysicae 37:143–151. https://doi.org/10.5194/angeo-37-143-2019
14. King C-Y (1978) Radon emanation on San Andreas Fault. Nature 1978 271:5645 271:516–519. https://doi.org/10.1038/271516a0
15. Külahci F, Inceöz M, Doğru M, et al (2009) Artificial neural network model for earthquake prediction with radon monitoring. Applied Radiation and Isotopes 67:212–219. https://doi.org/10.1016/J.APRADISO.2008.08.003
16. Külahcı F, Aközcan S, & OG-J of R, 2020 undefined (2020) Monte Carlo simulations and forecasting of Radium-226, Thorium-232, and Potassium-40 radioactivity concentrations. researchgate.net. https://doi.org/10.1007/s10967-020-07059-y
17. Külahcı F, Şen, Z., (2014) On the Correction of Spatial and Statistical Uncertainties in Systematic Measurements of 222Rn for Earthquake Prediction. Springer 35:449–478. https://doi.org/10.1007/s10712-013-9273-8
18. Langley RB Monitoring the Ionosphere and Neutral Atmosphere with GPS
19. Li M, Parrot M (2018) Statistical analysis of the ionospheric ion density recorded by DEMETER in the epicenter areas of earthquakes as well as in their magnetically conjugate point areas. Advances in Space Research 61:974–984. https://doi.org/https://doi.org/10.1016/j.asr.2017.10.047
20. Lindmark A, Rosen B (1985) Radon in soil gas — Exhalation tests and in situ measurements. Science of The Total Environment 45:397–404. https://doi.org/https://doi.org/10.1016/0048-9697(85)90243-8

21. Liu JY, Chen CH, Chen YI, et al (2010) A statistical study of ionospheric earthquake precursors monitored by using equatorial ionization anomaly of GPS TEC in Taiwan during 2001–2007. Journal of Asian Earth Sciences 39:76–80. https://doi.org/https://doi.org/10.1016/j.jseaes.2010.02.012
22. MILNE J (1910) The California Earthquake of April 18, 1906. Nature 1910 84:2128 84:165–166. https://doi.org/10.1038/084165a0
23. Muhammad A, Külahcı F, Salh H, Hama Rashid PA (2021) Long Short Term Memory networks (LSTM)-Monte-Carlo simulation of soil ionization using radon. Journal of Atmospheric and Solar-Terrestrial Physics 221:105688. https://doi.org/10.1016/j.jastp.2021.105688
24. Namgaladze AA, Zolotov O V, Karpov MI, et al (2012) Manifestations of the earthquake preparations in the ionosphere total electron content variations. Natural Science 4:848–855. https://doi.org/10.4236/NS.2012.411113
25. Nazaroff W, Nero A (1988) Radon and its decay products in indoor air
26. Nazaroff WW (1992) Radon transport from soil to air. Reviews of Geophysics 30:137–160. https://doi.org/10.1029/92RG00055
27. Pulinets S (2018) The Possibility of Earthquake Forecasting: Learning from nature. IOP Publishing Ltd 2018
28. Rikitake T (1968) Earthquake prediction. Earth-Science Reviews 4:245–282. https://doi.org/https://doi.org/10.1016/0012-8252(68)90154-2
29. Salh H, Külahcı F, Aközcan S (2021) A mobile simulation and ARIMA modeling for prediction of air radiation dose rates. Journal of Radioanalytical and Nuclear Chemistry 2021 328:3 328:889–901. https://doi.org/10.1007/S10967-021-07726-8
30. Schery SD, Gaeddert DH (1982) Measurements of the effect of cyclic atmospheric pressure variation on the flux of 222RN from the soil. Geophysical Research Letters 9:835–838. https://doi.org/10.1029/GL009I008P00835
31. Shah M, Tariq MA, Ahmad J, et al (2019) Seismo ionospheric anomalies before the 2007 M7.7 Chile earthquake from GPS TEC and DEMETER. Journal of Geodynamics 127:42–51. https://doi.org/https://doi.org/10.1016/j.jog.2019.05.004
32. Singh M, Kumar M, Jain R, Chatrath R (2019) Radon in ground water related to seismic events
33. Tariq MA, Shah M, Hernández-Pajares M, Iqbal T (2019) Pre-earthquake ionospheric anomalies before three major earthquakes by GPS-TEC and GIM-TEC data during 2015–2017. Advances in Space Research 63:2088–2099. https://doi.org/https://doi.org/10.1016/j.asr.2018.12.028
34. Thomas DM, Cotter JM, Holford D (1992) Experimental design for soil gas radon monitoring. Journal of Radioanalytical and Nuclear Chemistry Articles 161:313–323. https://doi.org/10.1007/BF02040478
35. Ulomov VI, Zakharova AI, Nauk NVU-DA, undefined 1967 The Tashkent earthquake of April 26, 1966, and its repeated shocks. mathnet.ru

36. Venkatanathan, N., Yang, YC. & Lyu, J. (2017) Observation of abnormal thermal and infrasound signals prior to the earthquakes: a study on Bonin Island earthquake M7.8 (May 30, 2015). *Environ Earth Sci* **76,** 228.
37. Viñas R, Eff-Darwich A, Soler V, et al (2007) Processing of radon time series in underground environments: Implications for volcanic surveillance in the island of Tenerife, Canary Islands, Spain. Radiation Measurements 42:101–115. https://doi.org/10.1016/j.radmeas.2006.07.002
38. Virk HS, Walia V (2001) Helium/radon precursory signals of Chamoli Earthquake, India. Radiation Measurements 34:379–384. https://doi.org/https://doi.org/10.1016/S1350-4487(01)00190-1
39. Viti M, Mantovani E, Cenni N, Vannucchi A (2013) Interaction of seismic sources in the Apennine belt. Physics and Chemistry of the Earth, Parts A/B/C 63:25–35. https://doi.org/https://doi.org/10.1016/j.pce.2013.03.005
40. Zhao Y, Nielsen CP, Lei Y, et al (2011) Quantifying the uncertainties of a bottom-up emission inventory of anthropogenic atmospheric pollutants in China. Atmospheric Chemistry and Physics 11:2295–2308. https://doi.org/10.5194/acp-11-2295-2011

Figures

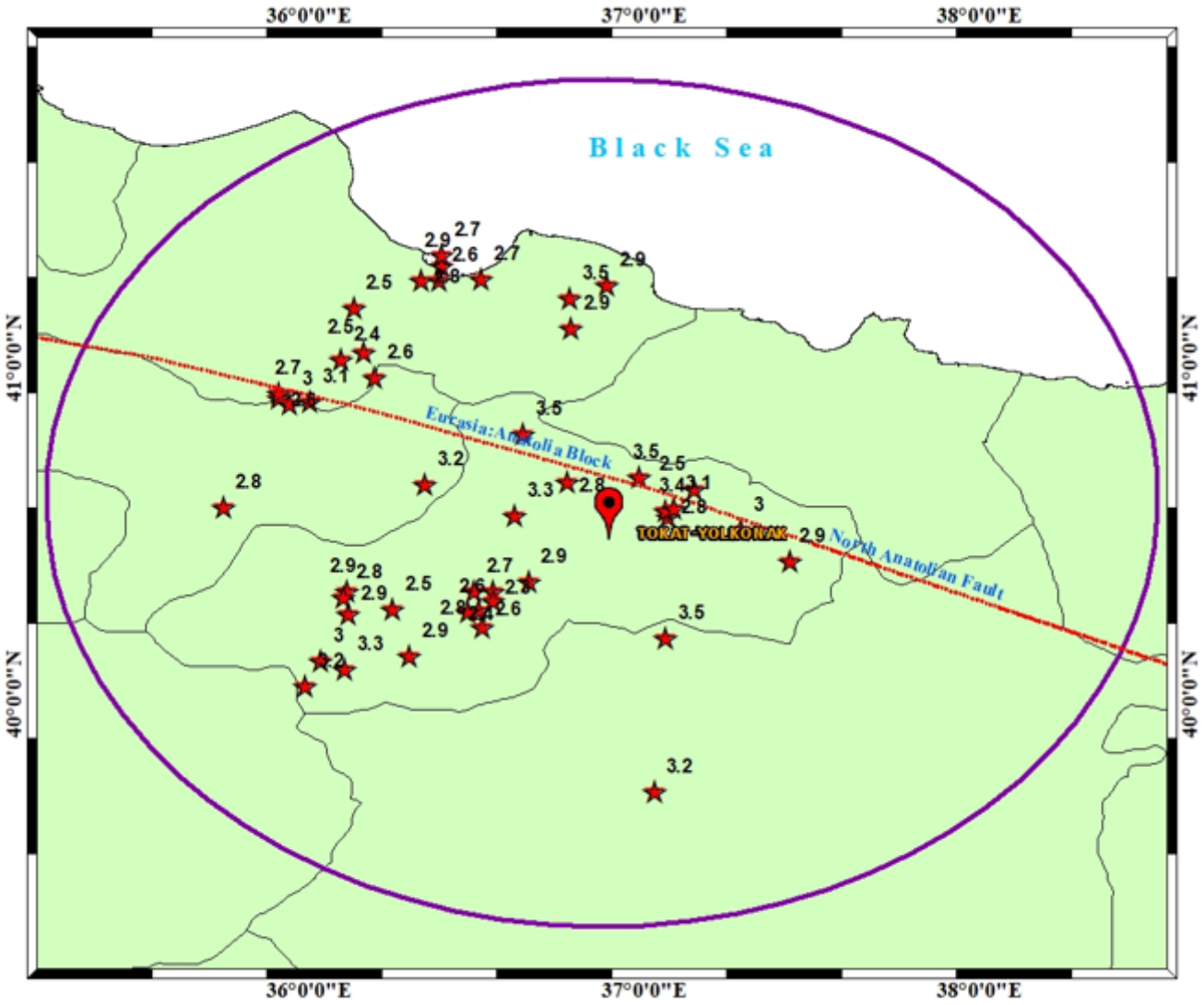

Figure 1

The exact location of the radon monitoring station and studied earthquakes along the NAF fault zones in Turkiye.

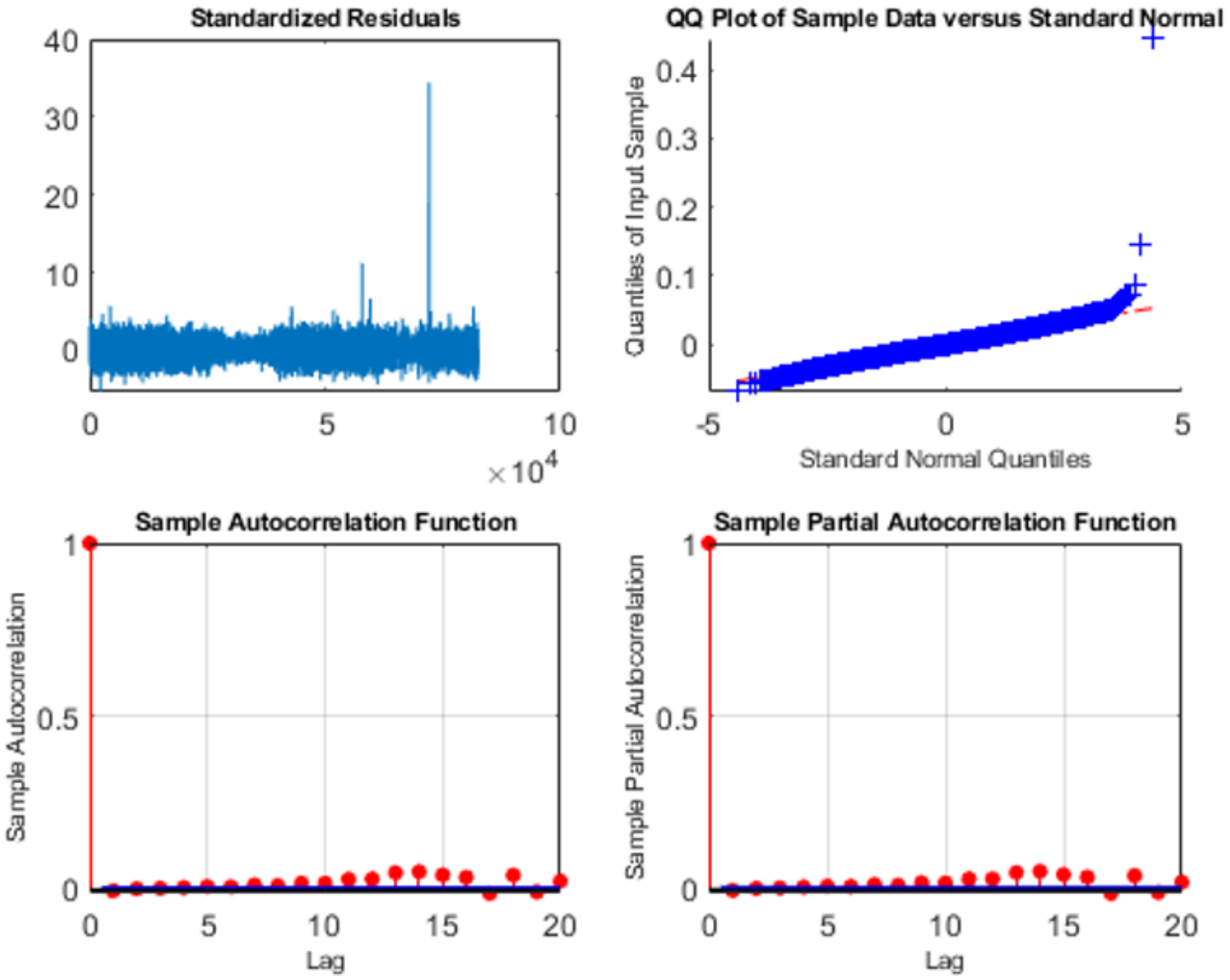

Figure 2

Partial autocorrelation function and autocorrelation function plots (lower part); the standardized residuals and the quantile-quantile of the ARIMA model residuals (upper part).

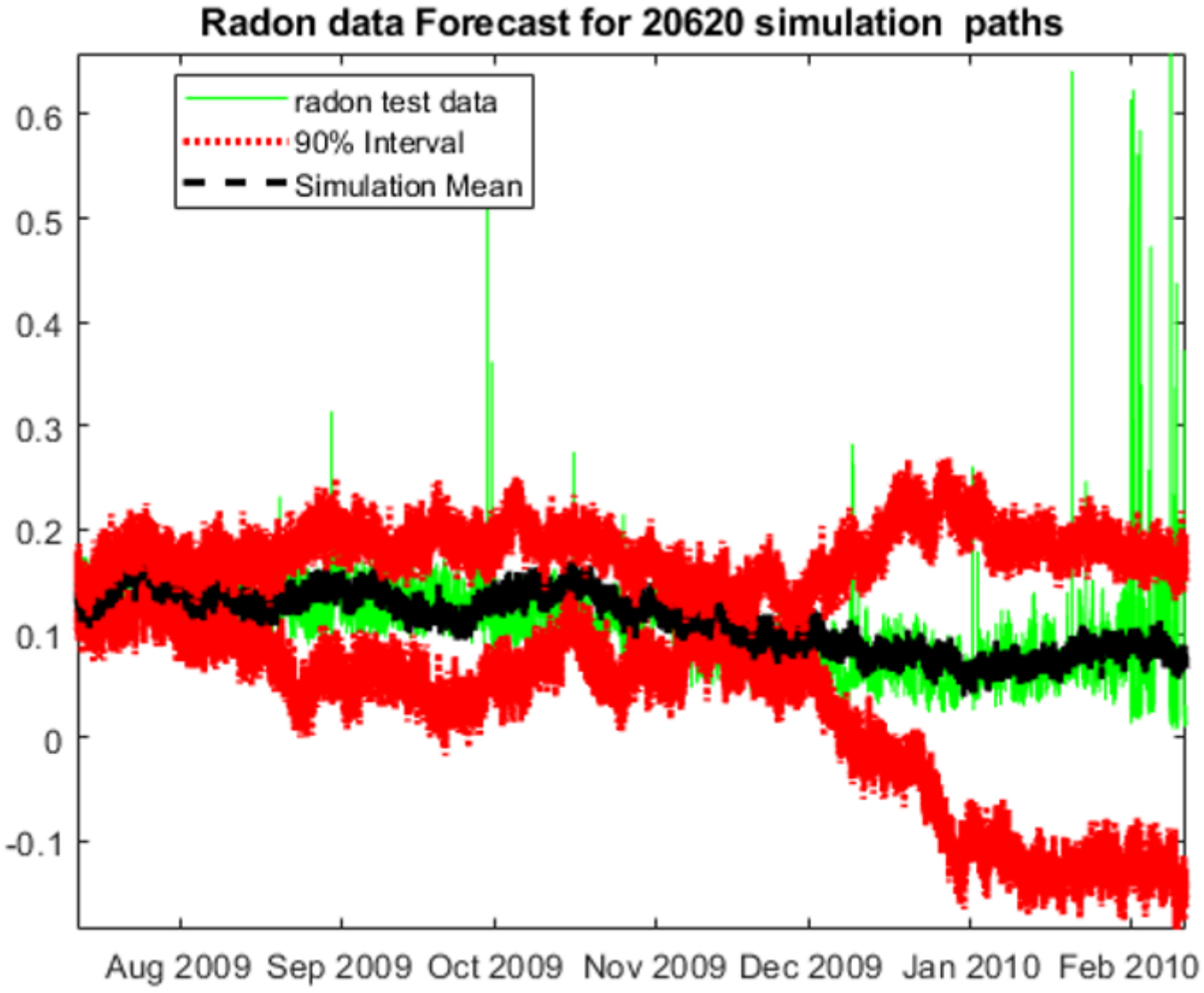

Figure 3

The mean of Monte Carlo Simulation Rn forecasts with lower and upper bounds.

Figure 4 The studied Rn time series data.

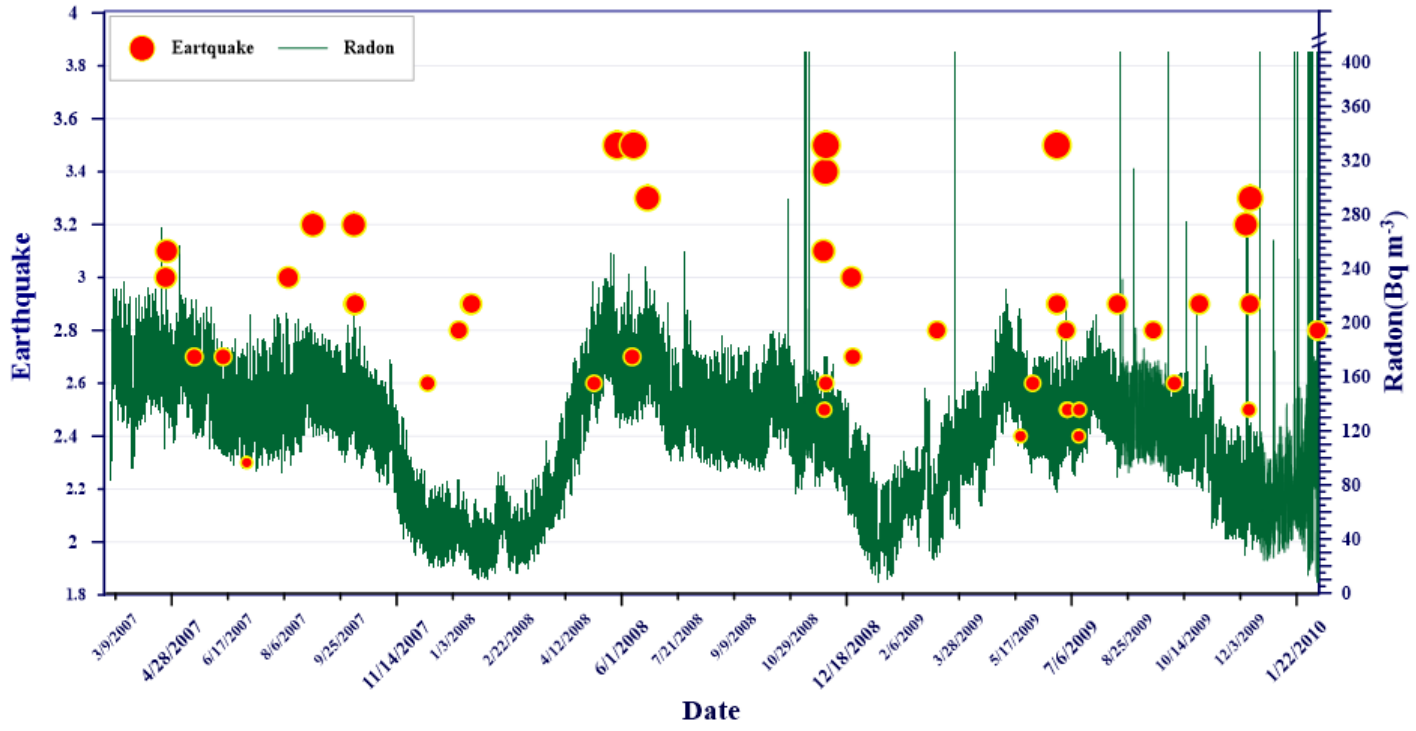

Figure 4

The variations of the radon concentration with soil temperature at (5, 10, 20, and 50 cm) depths.

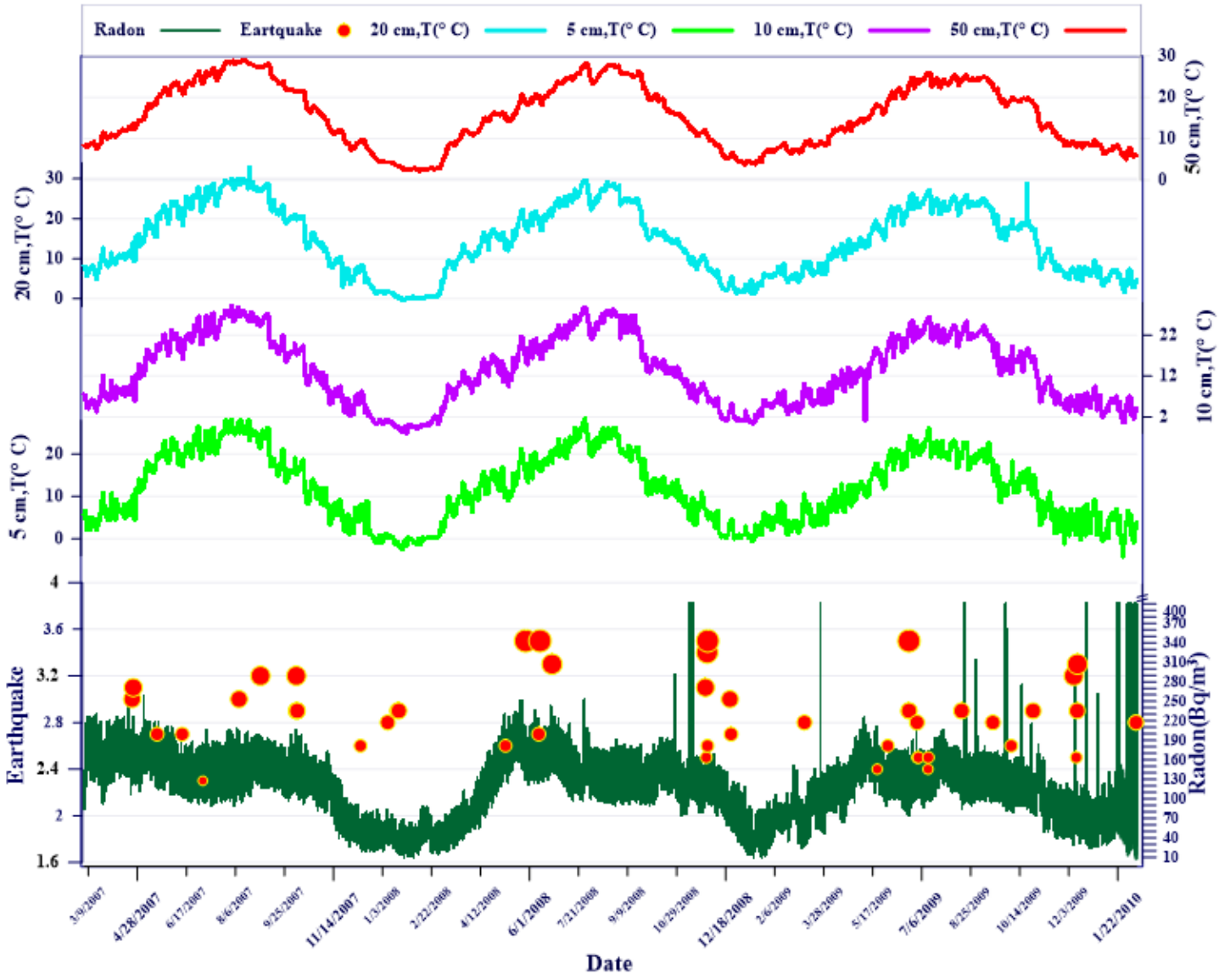

Figure 5

(a) The training and evaluation parts of the radon data with all earthquakes in the study area, **(b)** The MCS forecasted radon data.

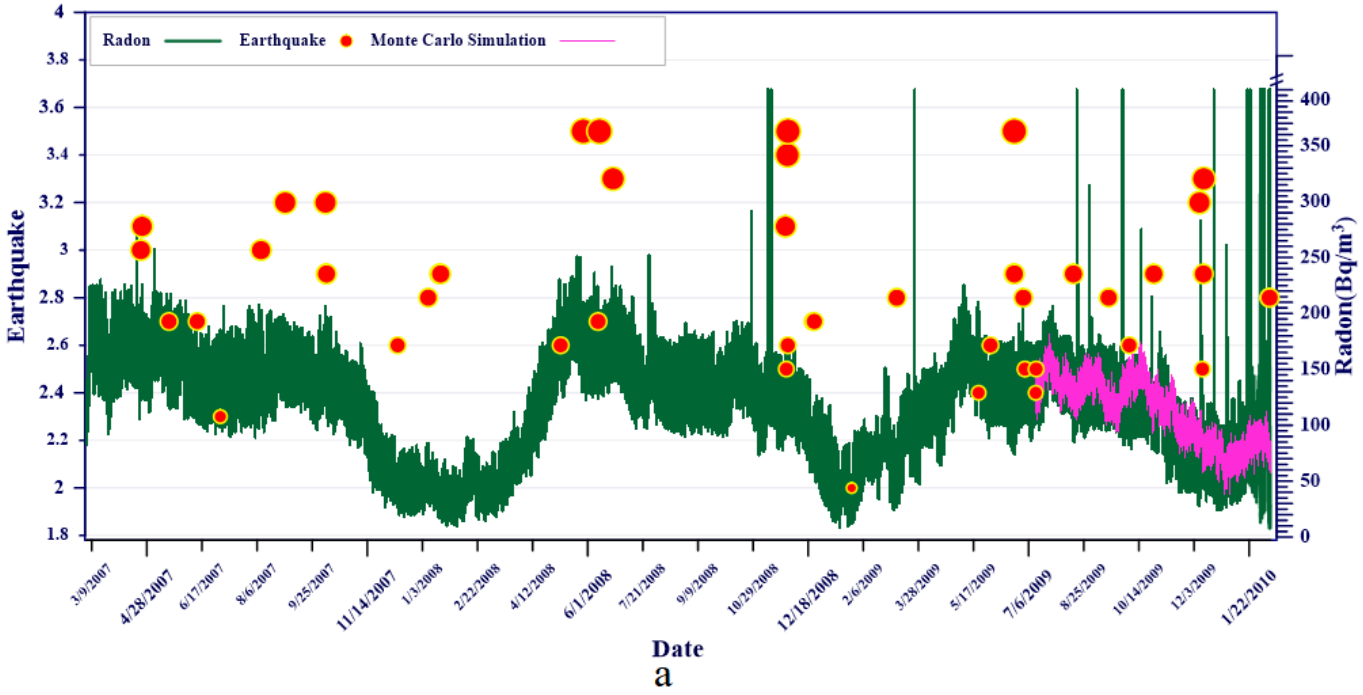

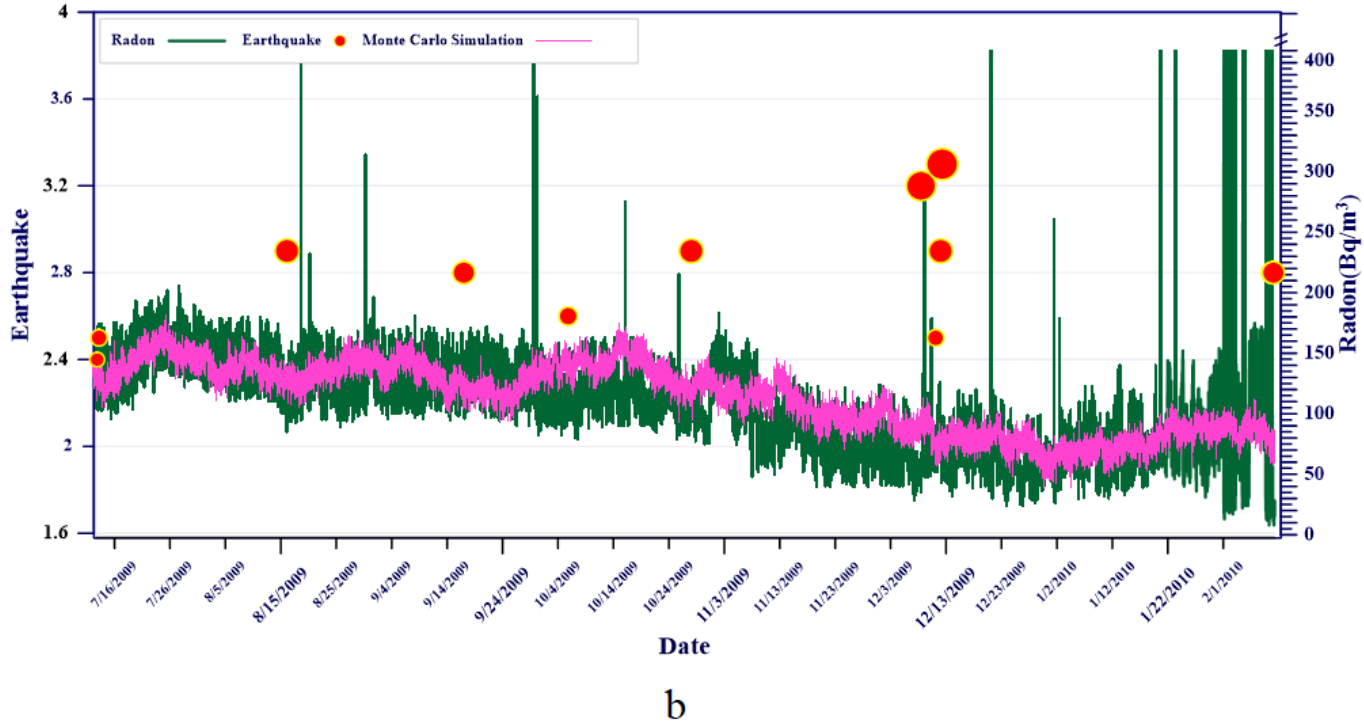

Figure 6

(a) The training and evaluation parts of the radon data with all earthquakes in the study area, **(b)** The MCS forecasted radon data.

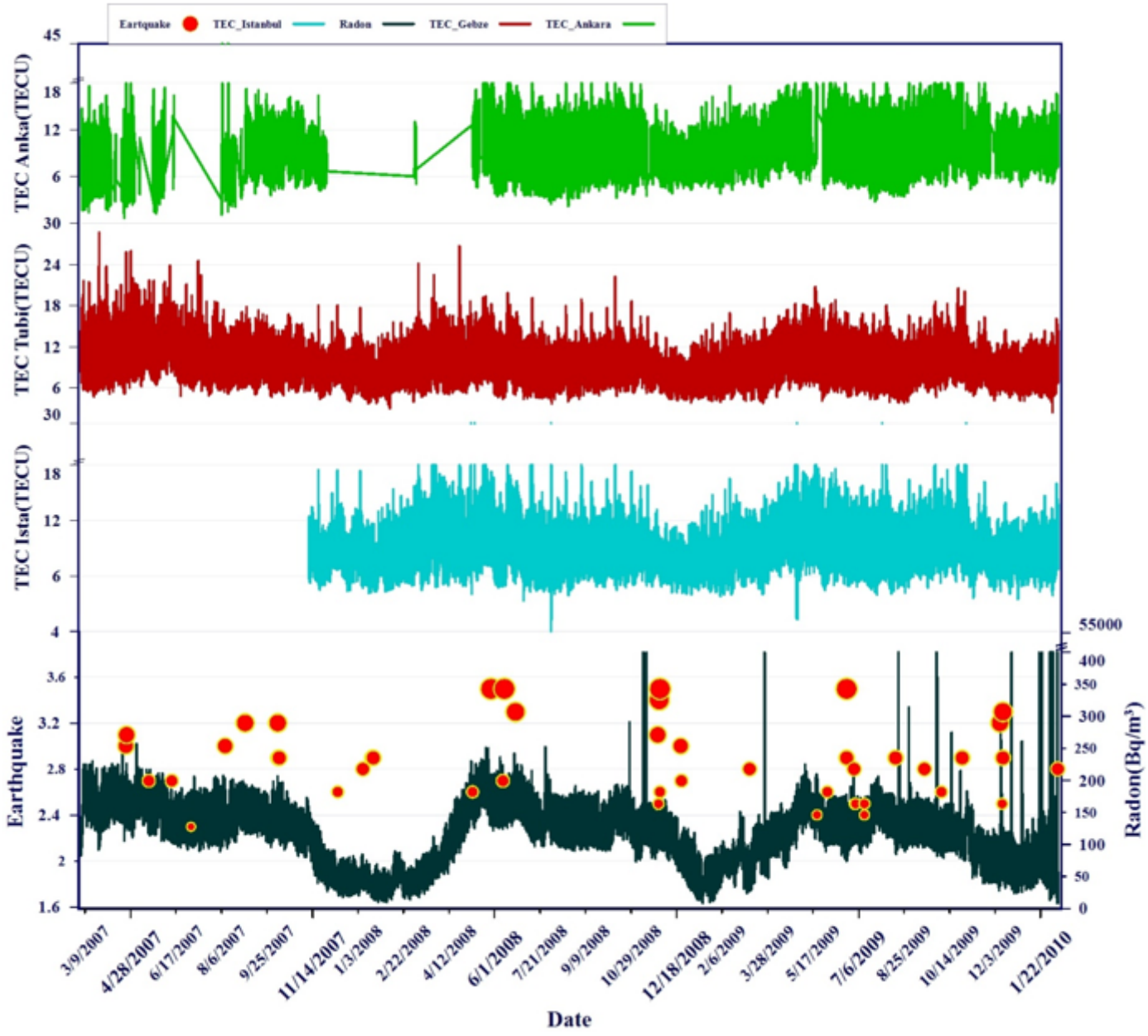

Figure 7

Radon time series, earthquake magnitude, and total electron content for three stations Tubi (Gebze), Ista (Istanbul), Anka (Ankara).

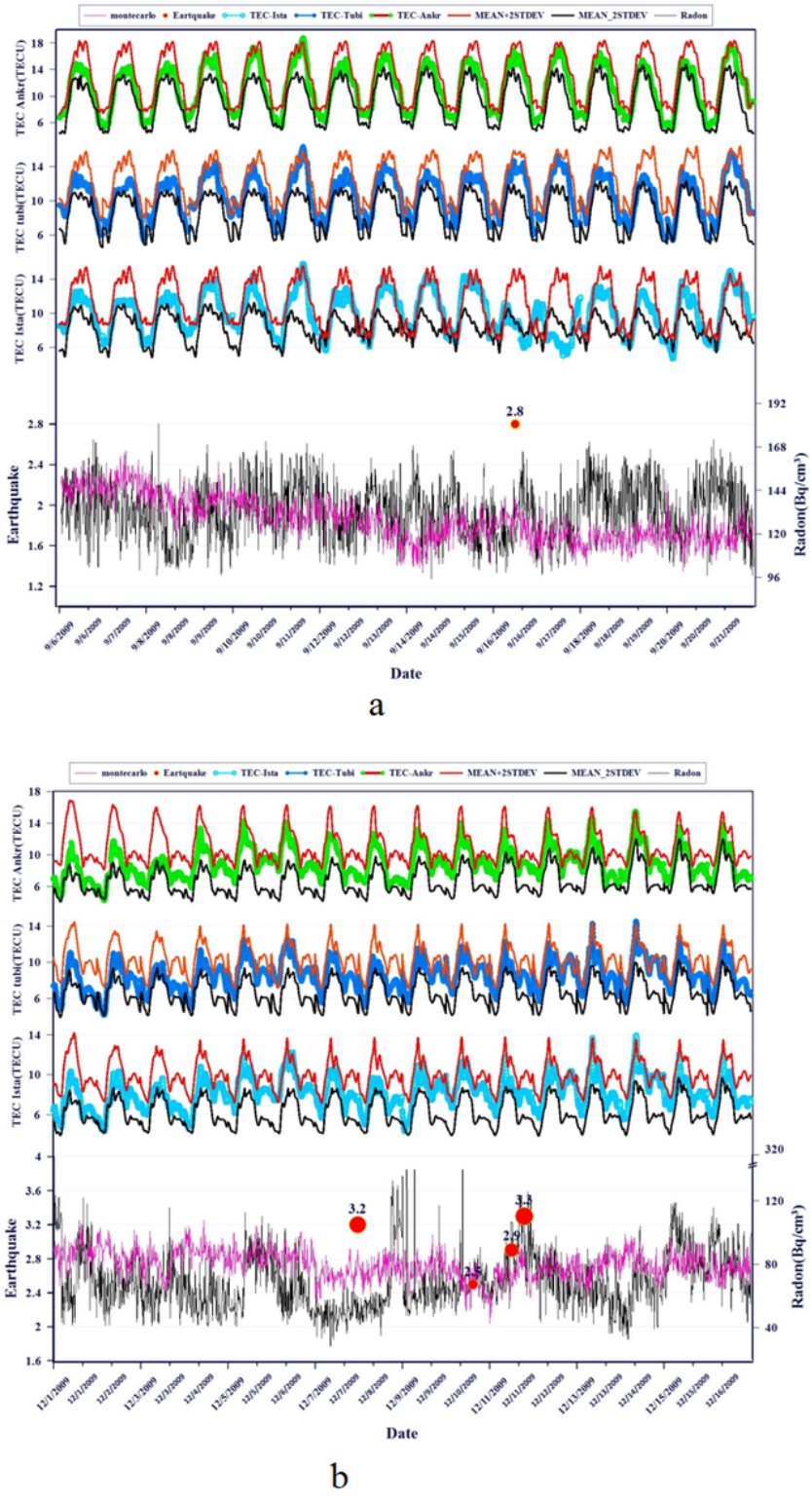

Figure 8

(a) TEC and radon variation before and after an earthquake M_L 2.9 on September 16, 2009 **(b)** TEC and radon variation before and after an earthquake M_L3.2 on December 7, 2009.

Supplementary Files

This is a list of supplementary files associated with this preprint. Click to download.

- Highlights.docx